Experimental Missile Pitch- and Roll-Damping Characteristics at Large Angles of Attack

Bob L. Uselton* and Leroy M. Jenke*
ARO, Inc., Arnold Air Force Station, Tenn.

Pitch- and roll-damping test mechanisms were developed for obtaining stability characteristics of high fineness ratio missiles at angles of attack up to 90 deg. Wind-tunnel tests were conducted on two missile configurations at Mach numbers 0.22 through 2.5. Mechanism evaluation tests showed that strut interference was not appreciable. The pitch-damping derivatives were found to be highly nonlinear functions of angle of attack, and the roll-damping and Magnus characteristics were very nonlinear with spin rate at high angles of attack and low Mach numbers. Large and erratic variations in side force and yawing moment with angle of attack and high autorotation characteristics also were found at the low Mach numbers.

Nomenclature

A = reference area (pitch-damping tests – 1.227 in.^{2}, roll-damping tests – 2.545 in.^{2})
C_{ℓ_0} = rolling-moment coefficient at $p=0$, $(L_{0_w}-L_{0_B})/q_\infty Ad$
C_{ℓ_p} = roll-damping coefficient, $\partial C_{\ell_T}/\partial[pd/2V_\infty]$, rad^{-1}
C_{ℓ_T} = total rolling-moment coefficient, $(L_{T_w}-L_{T_B})/q_\infty Ad$
C_m = pitching-moment coefficient, pitching moment/$q_\infty Ad$
C_{m_q} = pitching-moment coefficient due to pitch velocity, $\partial C_Y/\partial[pd/2V_\infty]$, rad^{-1}
C_{m_α} = pitching-moment coefficient due to angle of attack, $\partial C_m/\partial\alpha$, rad^{-1}
$C_{m_{\dot\alpha}}$ = pitching-moment coefficient due to rate of change of angle of attack, $\partial(C_m)/\partial(\dot\alpha d/2V_\infty)$, rad^{-1}
C_n = yawing (Magnus)-moment coefficient, yawing moment/$q_\infty Ad$
C_{n_p} = Magnus-moment spin derivative coefficient, $\partial C_n/\partial[pd/2V_\infty]$, rad^{-1}
C_Y = side (Magnus)-force coefficient, side force/$q_\infty A$
C_{Y_p} = Magnus-force spin derivative coefficient, $\partial C_Y/\partial[pd/2V_\infty]$, rad^{-1}
d = reference length, model diameter (pitch-damping tests – 1.25 in., roll-damping tests – 1.80 in.)
I_x = model moment of inertia about roll axis (see Fig. 1), slug-ft^2
I_y = model moment of inertia about pitch axis (see Fig. 1), slug-ft^2
L_{0B} = bearing static rolling moment at $p=0$, ft-lb
L_{0_w} = model-bearing system static rolling moment at $p=0$ (aerodynamic plus bearing), ft-lb
L_{TB} = total bearing rolling moment, ft-lb
L_{T_w} = model-bearing system total rolling moment (aerodynamic plus bearing), ft-lb
M_∞ = freestream Mach number
$p,\dot\phi$ = model spin rate, rad/sec
$pd/2V_\infty$ = spin rate parameter, rad
p_{ss} = model steady-state spin rate, rad/sec
q = pitching velocity, rad/sec
q_∞ = freestream dynamic pressure, lb/in.^{2} or lb/ft^2
Re_d = freestream Reynolds number based on model diameter
V_∞ = freestream velocity, ft/sec
X_p = distance from the model nose to the moment reference point (see Fig. 1), calibers
α = model angle of attack, deg, $\alpha=\alpha_s+\alpha_{pb}+\alpha_{trim}$
α_{pb} = effective sting prebend, deg, $\alpha_{pb}=\alpha_{sp}+\alpha_{st}$
α_s = tunnel sector pitch angle, deg
α_{sp} = angle of support sting with respect to centerline of tunnel sector, deg
α_{st} = angle of strut with respect to support sting centerline, deg
α_{trim} = angular deflection of cross-flexure balance because of static pitching moment, deg
$\dot\alpha$ = time rate of change of angle of attack, rad/sec
δ = model fin cant angle, deg
θ = oscillation amplitude, deg
ϕ = model roll position, deg or rad
$\dot\phi,p$ = model roll rate, rad/sec
ω = frequency of oscillation in pitch, rad/sec
$\omega d/2V_\infty$ = reduced frequency parameter, rad

Presented at the AIAA 9th Aerodynamic Testing Conference, Arlington, Texas, June 7-9, 1976 (in bound volume of Conference Papers, no paper number); submitted July 6, 1976; revision received Dec. 20, 1976.

Index categories: LV/M Aerodynamics; LV/M System and Component Ground Testing.

*Project Engineer, Aerodynamics Projects Branch, von Kármán Gas Dynamics Facility. Member AIAA.

Introduction

A CURRENT trend in missile development is toward large fineness ratio configurations which are highly maneuverable. The damping derivatives (pitch, yaw, and roll), especially on slender vehicles with fins, have a strong influence on the vehicle response at extreme maneuver conditions. Theoretical predictions at best apply only at low angles of attack, and since the new missiles are highly maneuverable, large angle-of-attack experimental data are desired for the computerized flight trajectory programs.

Two programs were initiated to develop the capability for obtaining high angle-of-attack aerodynamic data on current missile configurations. The first program[1,2] was a research effort directed toward developing a test mechanism for obtaining pitch-damping data, whereas the second program[2,3] developed a test mechanism for obtaining roll-damping, Magnus, and static stability data. Each test mechanism had an angle-of-attack range of approximately −10 to 90 deg and was designed for use in both the Arnold Engineering Development Center-von Kármán Gas Dynamics Facility Supersonic Wind Tunnel (A) ($M_\infty=1.5$ to 6.0) and the AEDC-Propulsion Wind-Tunnel Facility Aerodynamic Wind Tunnel (4T) ($M_\infty=0.2$ to 1.3).

The pitch-damping tests were conducted on the Basic Finner configuration at Mach number 2 utilizing the small-amplitude, free-oscillation technique. The roll-damping tests were conducted on Basic Finner and modified Basic Finner

configurations at Mach numbers of 0.22 through 2.5 utilizing the free-spin test technique. Data for both test programs were obtained at angles of attack from approximately −10 to 90 deg.

Apparatus

Models

Two stainless-steel configurations (Fig. 1) were designed and fabricated for these tests. One configuration, commonly referred to as the Basic Finner, consisted of a cone-cylinder with four rectangular fins. Three interchangeable sets of fins with cant angles of 0, 2.5, and 5 deg were fabricated. One additional configuration, the modified Basic Finner, also was tested during the roll-damping tests. It utilized the same body but with an ogive nose and four fins with a trapezoidal planform and zero-cant angle. Model diameter was 1.25 in. and 1.8 in. for the pitch- and roll-damping tests, respectively.

Test Mechanisms and Instrumentation

Pitch-Damping Mechanism and Instrumentation

The high-alpha pitch-damping test mechanism, designated 2.G High Alpha (Fig. 2), utilizes a small-amplitude, one-degree-of-freedom, cross-flexure balance which is supported by a strut and sting that can be adjusted manually to provide angles of attack ranging from −15 to 90 deg without introducing appreciable aerodynamic interference. A strain-gage bridge is located on the flexures to provide a voltage proportional to angular displacement. A pneumatic- and spring-operated locking device is provided to hold the model during injection into or retraction from the tunnel. Three balances, having flexure stiffnesses of 2.3, 23, and 49 in.-lb/deg and maximum amplitudes of ±4, ±3, and ±2 deg, respectively, are available for use with the test mechanism. The 49-in.-lb/deg balance was used during the present test.

An oscillating-air system was used to displace the model. The driving force was obtained from a high-pressure air supply which was adjusted to the pressure level necessary to overcome the damping moment. The model was oscillated by two air jets that were regulated by a remotely controlled servovalve oscillating at the natural frequency of the model and balance system. The driving force could be stopped abruptly by a solenoid valve and data recorded as the amplitude decreased.

Roll-Damping Mechanism

The 2.H High-Alpha missile roll-damping test mechanism (Fig. 3) is a free-spin system. A six-component moment balance (−71) is supported by a strut that can be set manually in 6-deg increments to provide various prebend angles. These manual settings, along with the tunnel pitch mechanism, provide an angle-of-attack range from −5 to 90 deg. The balance supports an adapter with three ball bearings and the model is mounted directly to the bearings. Roll-damping data are obtained as the model spins up (for models with canted fins) or as the model spins down after it is spun up by high-pressure air jets impinging on the fins. An air-operated brake is located on the front of the adapter and is used to stop model rotation. The maximum dynamic braking moment produced by the brake is 13.5 in.-lb; however, this possibly could be increased by using different braking materials. The brake, as well as a mechanical lock, can be used to obtain static-force coefficients at zero spin rate. The Basic Finner model also was tested with a straight-sting support[2,3] for the purpose of evaluating possible strut interference of the high-alpha mechanism.

The rotational speed, roll position, and roll direction are computed from the electrical pulses produced by a ring, with alternating reflective and nonreflective surfaces passing three internally mounted infrared-emitting diodes and

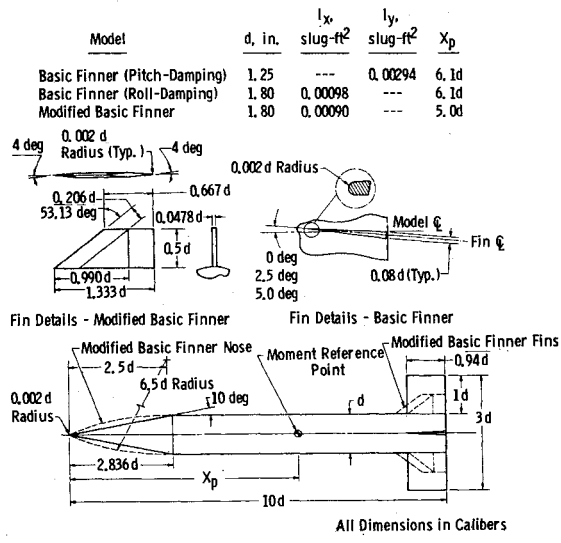

Fig. 1 Model details.

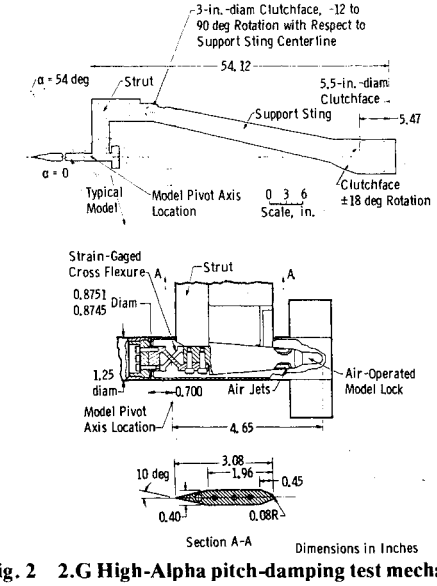

Fig. 2 2.G High-Alpha pitch-damping test mechanism.

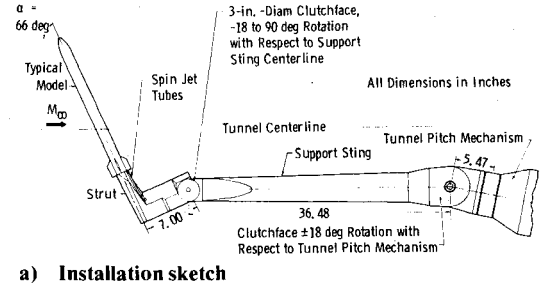

a) Installation sketch

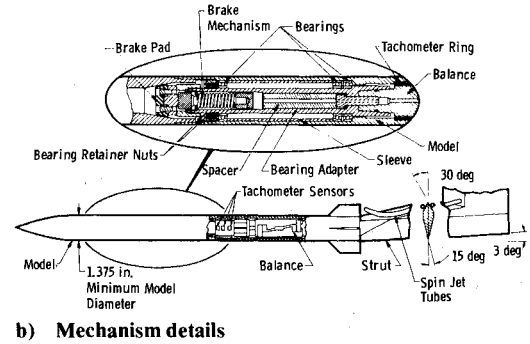

b) Mechanism details

Fig. 3 2.H High-Alpha missile roll-damping test mechanism.

Table 1 Test summaries

Pitch-damping tests ($M_\infty = 1.96$)		
$Re_d \times 10^{-5}$	$\omega d/2V_\infty \times 10^3$	α, deg
0.86	8.7	0 to 84
1.87	8.7	−12 to 86
Roll-damping tests		
M_∞	$Re_d \times 10^{-5}$	α, deg
0.22[a]	1.05	−5 to 83
0.60[b]	2.60	−5 to 90
0.90[b]	2.60	−5 to 90
1.15[b]	4.17	−5 to 90
1.50[b]	4.13	−5 to 65
1.76[b]	4.13	−5 to 90
2.49[a]	1.86	−5 to 90[c]
2.50[b]	4.10	−5 to 90
2.50[a]	5.97	−5 to 43[c]

[a]Basic Finner.
[b]Modified Basic Finner (data[3] also were obtained at $M_\infty = 1.30$, 2.00, and 2.25).
[c]Data[2,3] also were obtained with a straight sting for $\alpha = -5$ to 20 deg.

phototransistors. The mechanism is designed for spin rates up to 12,000 rpm and normal force loads of 300 lb.

Test Facilities

Tunnel A is a continuous, closed-circuit, variable-density wind tunnel with an automatically driven flexible-plate-type nozzle and a 40×40-in. test section. The tunnel can be operated at Mach numbers from 1.5 to 6.0 at maximum stagnation pressures from 29 to 200 psia, respectively, and stagnation temperatures up to 750°R ($M_\infty = 6$). Although Tunnel A is primarily a supersonic tunnel, it also can be operated subsonically from Mach numbers 0.2 to 0.8.

Tunnel 4T is a closed-circuit, continuous-flow, variable-density tunnel capable of being operated at Mach numbers from 0.20 to 1.30. At all Mach numbers, the stagnation pressure can be varied from about 2 to 27 psia. The test section is 48-in. square and 150-in. long with perforated, variable porosity (0.5 to 10%) walls.

Procedure

Test Conditions

The nominal wind-tunnel test parameters at which the pitch- and roll-damping data were obtained are presented in the test summaries of Table 1. Pitch-damping data normally were obtained for oscillation amplitudes from ±1.4 to ±0.6 deg. The pitch data are presented for oscillation amplitudes (θ) of ±1 deg. Roll-damping data also were obtained at other intermediate Mach numbers, and these results can be found in Ref. 3.

Test and Data Reduction Procedures

Complete documentation of the test procedure, data reduction, and error analysis may be found in Refs. 1-3.

Results and Discussion

Pitch-Damping Data

The pitch-damping and static stabililty derivatives are presented in Fig. 4 as a function of angle of attack for the Basic Finner configuration for Reynolds numbers, based on model diameter, of 0.86×10^5 and 1.87×10^5. The different symbols in Fig. 4 indicate the data that were obtained with one particular strut and support sting arrangement. In general, the data overlap from the different strut-sting combinations was good for both the static and dynamic derivatives. The fact that the data overlap was good gives a high confidence level that the strut-support sting interference was not appreciable for angles of attack greater than 6 deg, where data overlap started (Fig. 4b). The possibility existed at

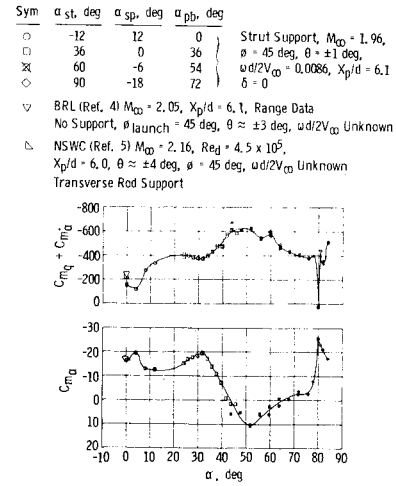

a) $Re_d = 0.86 \times 10^5$

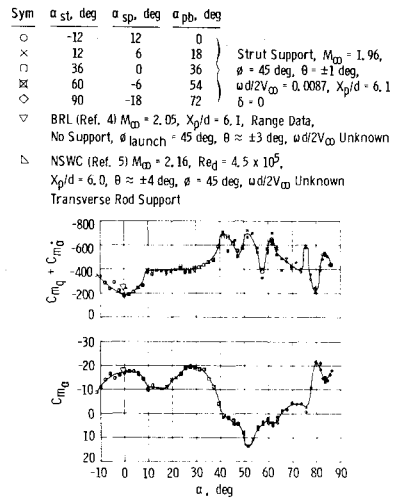

b) $Re_d = 1.87 \times 10^5$

Fig. 4 Pitch-damping and static stability derivatives as a function of angle of attack for the Basic Finner model.

low angles of attack that the strut would cause interference until the angle of attack was sufficient to hide the strut behind the model. However, the interference, if existing, appeared to be a minimum, since the pitch-damping and static stability data were fairly symmetrical about $\alpha = 0$ and also showed fairly good agreement at $\alpha = 0$ with BRL data free of any support effects[4] and with transverse rod support NSWC data[5] (Figs. 4a and b). The present data were small-amplitude, local-effective derivatives,[6] whereas the BRL and NSWC data are large-amplitude effective data.

The data in Fig. 4 showed the derivatives to be a highly nonlinear function of angle of attack. It is of interest to note that, for angles of attack above 40 deg at the higher Reynolds number, $Re_d = 1.87 \times 10^5$ (Fig. 4b), the dynamic measurements exhibited more scatter as compared to lower angle-of-attack data, and the damping derivatives also became highly nonlinear and oscillatory. A possible explanation for these unsteady dynamic data is an unsteady vortex system and/or the interaction between the shed vortices and fins. It is documented by Gowen and Perkins[7] that as the angle of attack is increased, the vortex system on the leeward side changes from a steady symmetric pair to a steady asymmetric configuration of two or more vortices and then to an unsteady asymmetric system at the high angles of attack. Gowen and Perkins also were able to obtain a correlation for several models defining the region of unsteady wake flow as a function of nose fineness ratio and apex angle. According to

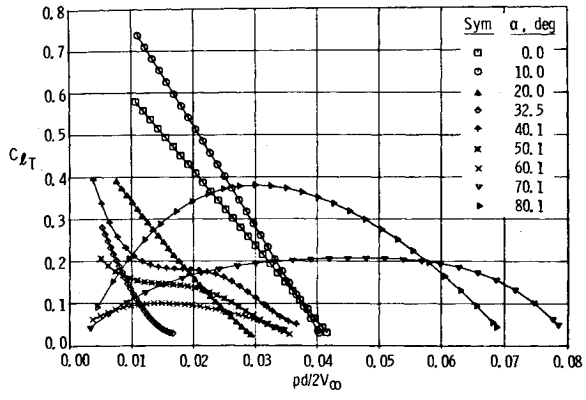

a) $M_\infty = 0.22$, $Re_d = 1.05 \times 10^5$, spin up with $\delta = 5$ deg

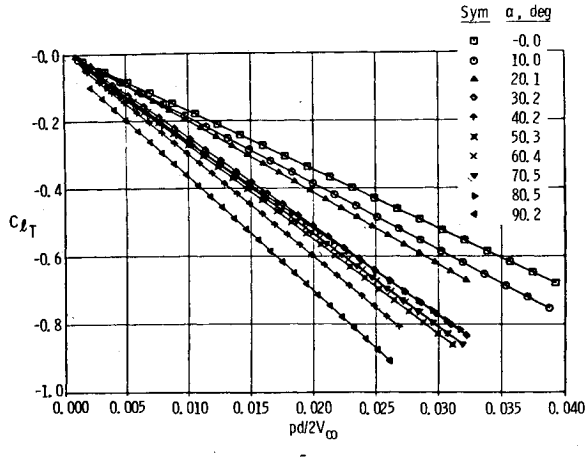

b) $M_\infty = 2.50$, $Re_d = 1.86 \times 10^5$, spin down with $\delta = 0$ deg

Fig. 5 Variation of C_{ℓ_T} with spin rate parameter for the Basic Finner model.

the correlation, the borderline to the unsteady conditions begins at $\alpha \approx 35$ deg for the Basic Finner model. This seems to be in agreement with the beginning of the unsteady data in Fig. 4b. In addition, the repeatability of the high-angle-of-attack damping measurements at the lower Reynolds number (Fig. 4a) was found to be better than that at the largest Reynolds number (Fig. 4b). Normally the reverse of this is true, since the measured damping moment is larger at the higher Reynolds number. The answer to this may be that the unsteadiness of the vortices may be more pronounced at the higher Reynolds number.

As mentioned in the previous paragraph, concerning Fig. 4, there were some small Reynolds number effects at the high angles of attack which were pertinent in analyzing the unsteady nonlinear damping data; however, over the angle-of-attack range (except at $\alpha \approx 80$ deg) there were essentially no consistent effects of Reynolds number for the limited Reynolds number range investigated. At $\alpha \approx 80$ deg, model damping decreased sharply for both Reynolds numbers. The lower Reynolds number ($Re_d = 0.86 \times 10^5$) data actually showed the model to be slightly unstable. However, model damping on each side of this "instantaneous peak" was quite high. The static stability derivative C_{m_α} also showed a spike at $\alpha \approx 80$ deg for both Reynolds numbers.

Roll-Damping Data

The variations of the total rolling-moment coefficient C_{ℓ_T} with spin rate for the Basic Finner model are presented in Fig. 5. At Mach number 0.22 (Fig. 5a), the variation of C_{ℓ_T} was a linear function of roll rate only at small angles of attack ($\alpha <$ 20 deg). At the higher angles of attack, the variations were very nonlinear and as a result, $C_{\ell_p} = \partial C_{\ell_T} / \partial [pd/2V_\infty]$ varied

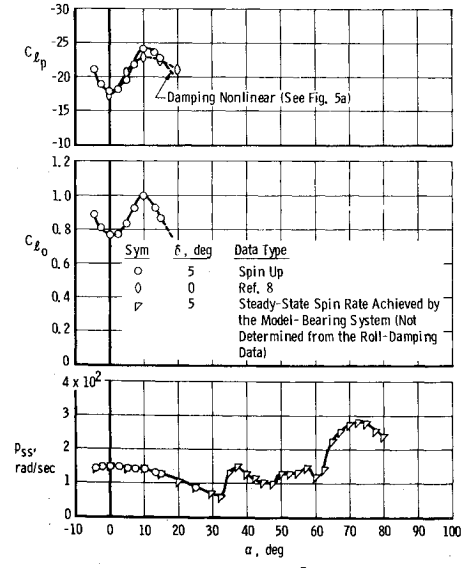

a) $M_\infty = 0.22$, $Re_d = 1.05 \times 10^5$

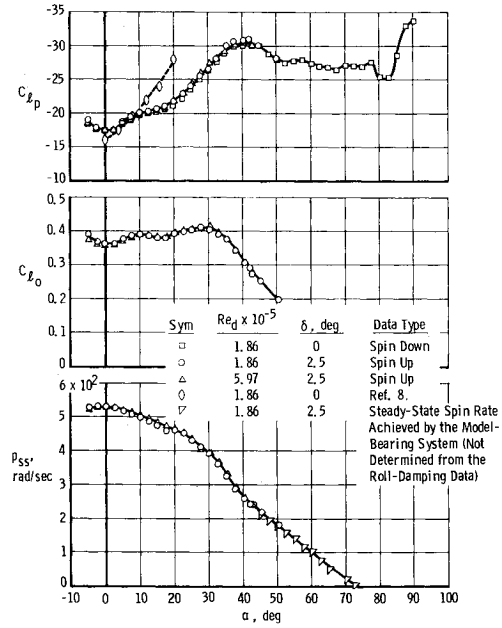

b) $M_\infty = 2.5$, $Re_d = 1.86 \times 10^5$

Fig. 6 Roll-damping characteristics of the Basic Finner model.

with $pd/2V_\infty$ and cannot be used in the traditional manner. Therefore, in this documentation values of C_{ℓ_p} will be presented only for linear or nearly linear damping. At Mach number 2.5 (Fig. 5b) the variation of C_{ℓ_T} was linear at all angles of attack.

The roll-damping characteristics of the Basic Finner model at $M_\infty = 0.22$ and 2.50 are presented in Fig. 6 as a function of angle of attack. At $M_\infty = 0.22$ the damping was nonlinear for $\alpha > 17.5$ deg, and the agreement of the linear data with results obtained by Regan[8] was good. The rolling moment at zero spin (C_{ℓ_0}) reached a maximum at $\alpha = 10$ deg and 30 deg for $M_\infty = 0.22$ and 2.50, respectively. The model exhibited an autorotation characteristic at the high angles of attack. At $\alpha \approx 75$ deg the steady-state spin rate was nearly double the steady-state spin rate at $\alpha = 0$. The results in Fig. 6b for $M_\infty = 2.5$ showed that there was excellent agreement in C_{ℓ_p} values for the spin-up data ($\delta = 2.5$ deg) and the spin-down data ($\delta = 0$). It should be noted that the two sets of data were recorded during different tunnel test entries, thereby indicating good data repeatability. There was also fair

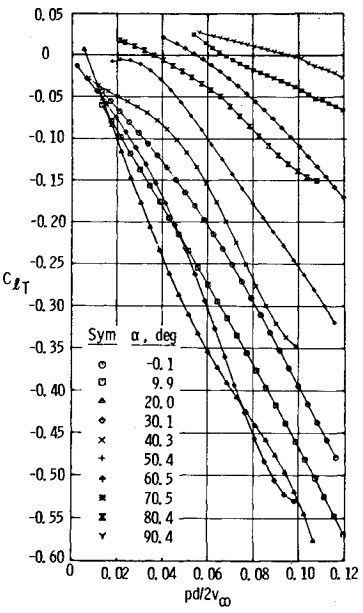

Fig. 7 Variation of C_{ℓ_T} with rate parameter for the Modified Basic Finner model ($M_\infty = 0.60, Re_d = 2.60 \times 10^5$).

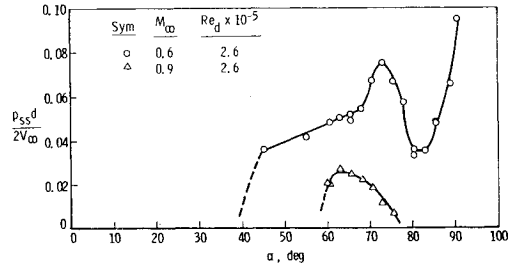

Fig. 8 Autorotation characteristics of the Modified Basic Finner model.

agreement with the test results obtained by Regan for $\alpha < 15$ deg.

The variations of the total rolling-moment coefficient C_{ℓ_T} with spin rate for the modified Basic Finner are presented in Fig. 7 for $M_\infty = 0.6$. The results for the higher Mach numbers are not presented; however, their effects are discussed. The data from Ref. 3 showed that C_{ℓ_T} was very nonlinear at the lower Mach numbers ($M_\infty \leq 0.9$) and that some nonlinearities even existed at the supersonic Mach numbers ($M_\infty \leq 1.5$). In addition, for $M_\infty \leq 0.9$, the value of C_{ℓ_T} was zero at spin rates other than zero (e.g., $M_\infty = 0.6$, Fig. 7). Therefore, the model will autorotate at these conditions. Figure 8 presents the spin rates at which the modified Basic Finner model (corrected for bearing moments) would autorotate. At $M_\infty = 0.6$ the model began to autorotate on the bearing system at $\alpha \approx 45$ deg and reached a maximum value ($pd/2V_\infty = 0.095$, $p \approx 860$ rad/sec) at $\alpha = 90$ deg. At $M_\infty = 0.9$ the autorotation on the bearing system started at $\alpha \approx 60$ deg and reached a maximum value ($pd/2V_\infty = 0.026$, $p \approx 340$ rad/sec) at $\alpha = 63$ deg and did not autorotate above 78 deg.

The variations of C_{ℓ_p} with angle of attack for the modified Basic Finner model are presented in Fig. 9. As noted before, only the results for linear damping are presented with the exception of slightly nonlinear values at lower angles of attack ($\alpha < 30$ deg). The results showed that as the Mach number increased, the range of angles of attack for which the damping was linear also increased. The dashed line fairing indicates regions of nonlinear damping as well as the general indicated data trend.

The approximate region of nonlinear roll damping for the modified Basic Finner model as obtained from Ref. 3 is indicated in Fig. 10. The data showed that nonlinear damping occurred at low Mach numbers ($M_\infty \leq 1.5$) and high angles of attack ($\alpha \gtrsim 17$ deg).

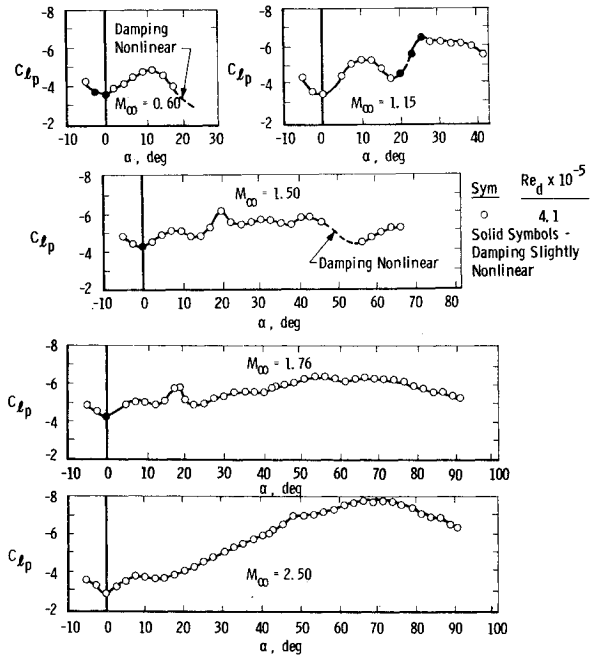

Fig. 9 Variation of C_{ℓ_p} with angle of attack for the Modified Basic Finner model, linear damping.

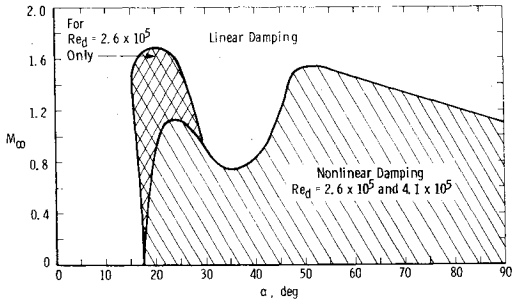

Fig. 10 Approximate regions of nonlinear damping, Modified Basic Finner model.

Although the mechanism was designed primarily to obtain roll-damping data, the system records the forces and moments acting on the model as the spin rate varies. Figure 11 presents the Magnus force (side force) and Magnus moment (yawing moment) characteristics of the Basic Finner Model. The magnitude of both C_Y and C_n increased with spin rate at $M_\infty = 2.5$ (Fig. 11b) in the typical manner. The maximum values were obtained at approximately 40 deg angle of attack. At $M_\infty = 0.22$ (Fig. 11a), the variations with spin rate are shown clearly; however, at some of the angles of attack ($\alpha \approx 60$ deg) large values of C_Y and C_n were indicated at zero spin rate. These forces were probably the result of the asymmetric vortex system which was discussed earlier.

The directional stability characteristics of the Basic Finner model rotating at spin rates of approximately 33 and 100 rad/sec for Mach numbers 0.22 and 2.5, respectively, are presented in Fig. 12. For these spin rates, the Magnus forces were small and the values should be representative of values occurring at $p = 0$. Note the large and abrupt changes in both C_Y and C_n with small changes in angle of attack, indicating a strong influence of the vortex system. Similar effects previously were shown to occur also for the modified Basic Finner at $M_\infty \leq 1.5$ (see Ref. 3). Both configurations, however, showed systematic trends for the $M_\infty > 1.5$, and both C_Y and C_n approached zero as the spin rate approached zero.

The Magnus-force and moment-spin derivative coefficients of the Basic Finner model are presented in Fig. 13 as a func-

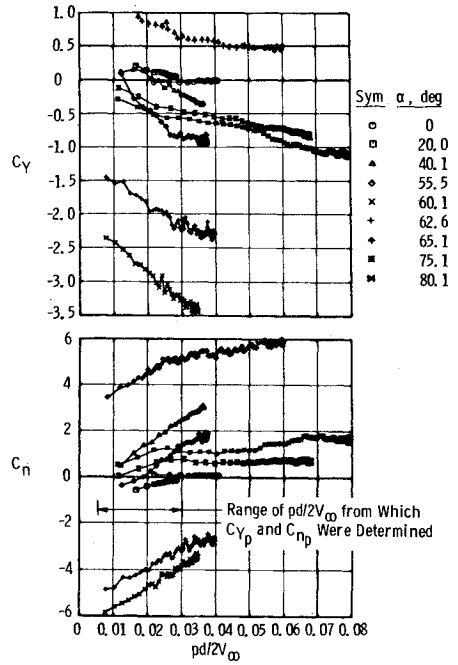

a) $M_\infty = 0.22$, $Re_d = 1.05 \times 10^5$

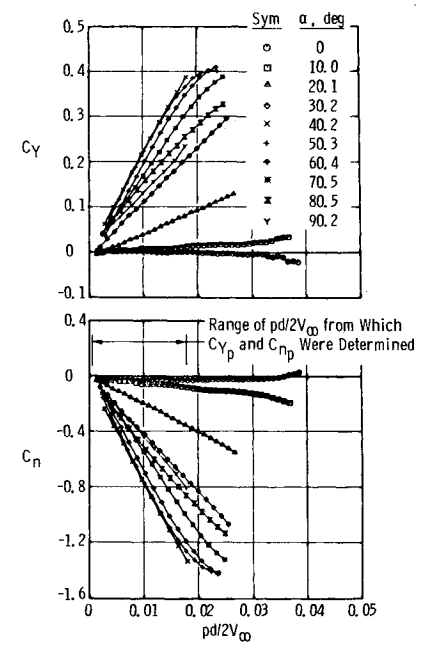

b) $M_\infty = 2.50$, $Re_d = 1.86 \times 10^5$

Fig. 11 Magnus-force and moment characteristics of the Basic Finner model.

tion of angle of attack. At $M_\infty = 0.22$, there were erratic variations in the data for $\alpha > 30$ deg. Two items that could contribute to these variations are the relatively small range of spin rates which results in only short segments of the data being fitted (see Fig. 11a) and the unsteady vortex system. Although there were erratic variations, the data showed a definite trend in the magnitude of both C_{Y_p} and C_{n_p} as the angle of attack increased. The maximum values of both C_{Y_p} and C_{n_p} occurred at $\alpha \approx 50$ deg. At $M_\infty = 2.5$ (Fig. 13b) the variations of C_{Y_p} and C_{n_p} with α were very smooth, and the agreement of the values obtained from the spin-down data with the values obtained from the spin-up data was excellent. It should be noted that the signs of both parameters changed as the Mach number increased from 0.22 to 2.50. The values of C_{Y_p} and C_{n_p} for the modified Basic Finner (see Ref. 3) also

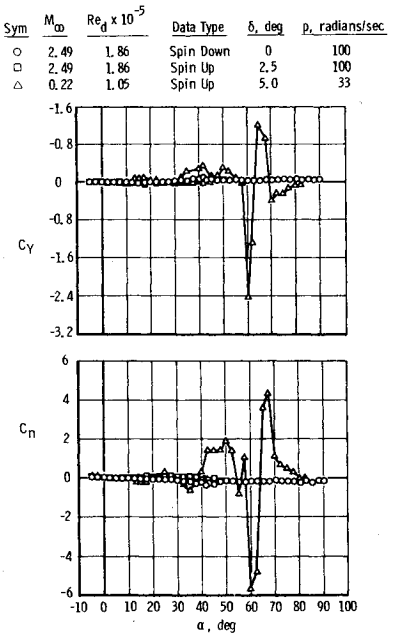

Fig. 12 Variation in directional stability with angle of attack for the Basic Finner model.

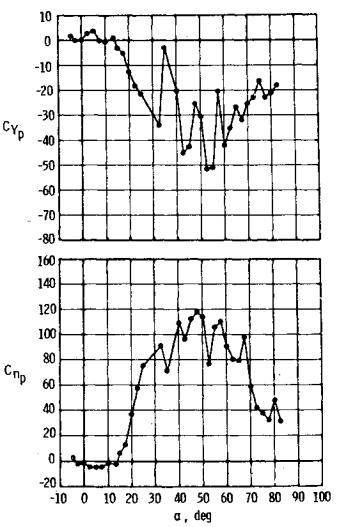

a) $M_\infty = 0.22$, $Re_d = 1.05 \times 10^5$

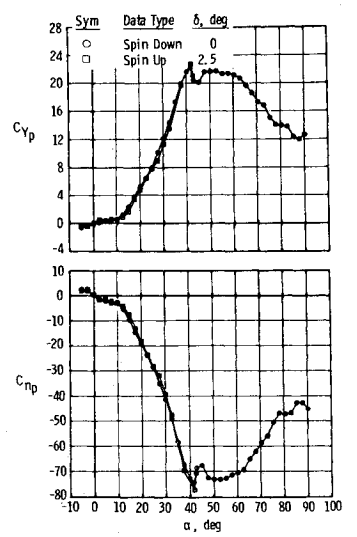

b) $M_\infty = 2.50$, $Re_d = 1.86 \times 10^5$

Fig. 13 Variation of C_{Y_p} and C_{n_p} with angle of attack for the Basic Finner model.

showed large variations with angle of attack and for $M_\infty \leq 1.3$ changed signs several times as angle of attack increased from 0 to 90 deg. The static longitudinal stability and axial force characteristics of both models also were recorded, and the results may be found in Refs. 2 and 3.

Conclusions

Wind-tunnel tests were conducted with newly developed high-alpha pitch- and roll-damping test mechanisms. Data were obtained on two missile configurations at Mach numbers 0.22 through 2.5 for angles of attack from -10 to 90 deg. Conclusions based on the test results are as follows:

1) The pitch-damping and static-stability derivatives can be measured accurately at angles of attack up to 90 deg.

2) The pitch-damping and static-stability derivatives at Mach number 2 are nonlinear functions of angle of attack and except for one "instantaneous peak" at 80 deg, the Basic Finner model is dynamically stable in pitch.

3) Roll-damping characteristics of the Basic Finner model obtained in these tests are in agreement with existing data, and there was no effect produced by the test mechanism strut or the spin jet tubes at Mach number 2.5 and angles of attack below 20 deg.

4) The roll-damping characteristics vary considerably with Mach number and angle of attack, and the rolling moment is generally nonlinear with spin rate at large angles of attack (greater than 20 deg) and low Mach numbers (less than 1.5).

5) The modified Basic Finner with zero canted fins autorotated at high angles of attack (greater than 45 deg) at Mach numbers 0.6 and 0.9.

6) Magnus force and moment characteristics are very nonlinear with spin rate for Mach number less than 1.76. Large side forces and yawing moments also are present at zero spin rate at the same Mach numbers.

The results obtained in the roll-damping study indicate the potential problem of maintaining roll control of a missile of this type if its trajectory includes high angle-of-attack maneuvers which take place at the lower Mach numbers. The presence of the large side loads also would be a potential problem. The nonlinearity of the rolling moment means that the data cannot be used in the normal manner in trajectory programs and that current preliminary design trajectories being computed without these parameters could have gross errors.

Acknowledgment

The work reported herein was conducted by the Arnold Engineering Development Center (AEDC), Air Force Systems Command (AFSC). The results presented herein were obtained by personnel of ARO, Inc., contract operator of AEDC. The pitch-damping tests were sponsored by AEDC, AFSC. The roll-damping tests were sponsored by the Air Force Flight Dynamics Laboratory (AFFDL), AFSC.

References

[1] Uselton, B. L. and Uselton, J. C., "Test Mechanism for Measuring Pitch-Damping Derivatives of Missile Configurations at High Angles of Attack," AEDC-TR-75-433 (ADA009865), May 1975.

[2] Uselton, B. L. and Jenke, L. M., "Test Mechanisms for Obtaining Dynamic Stability Characteristics of High Fineness Ratio Bodies at Angles of Attack up to 90 Deg," *Proceedings of the AIAA 9th Aerodynamic Testing Conference*, Arlington, Texas, June 7-9, 1976, pp. 76-90.

[3] Jenke, L. M., "Experimental Roll-Damping, Magnus, and Static Stability Characteristics of Two Slender Missile Configurations at High Angles of Attack (0 to 90 Deg) and Mach Numbers 0.2 Through 2.5," AEDC-TR-76-58, 1976.

[4] MacAllister, L. C., "The Aerodynamic Properties of a Simple Non-Rolling Finned Cone-Cylinder Configuration Between Mach Numbers 1.0 and 2.5," Ballistics Research Laboratory, Rept. 934, May 1955.

[5] Shantz, I. and Groves, R. T., "Dynamic and Static Stability Measurements of the Basic Finner at Supersonic Speeds," NAVORD Rept. 4516, Jan. 1960.

[6] Uselton, J. C. and Uselton, B. L., "Validity of Small Amplitude Oscillation Dynamic-Stability Measurement Technique," *Journal of Spacecraft and Rockets*, Vol. 13, No. 5, May 1976, pp. 266-270.

[7] Gowen, F. E. and Perkins, E. W., "A Study of the Effects of Body Shape on the Vortex Wakes of Inclined Bodies at a Mach Number of 2," NACA RM A53117, Dec. 1953.

[8] Regan, F. J., "Roll-Damping Moment Measurements for the Basic Finner at Subsonic and Supersonic Speeds," NAVORD Rept. 6652, June 1964.